Design of a superpositively charged enzyme: human carbonic anhydrase II variant with ferritin encapsulation and immobilization

*Joshua A. Bulos, Rui Guo, Zhiheng Wang, Maegan A. DeLessio, Jeffery G. Saven, Ivan J. Dmochowski**

Department of Chemistry, University of Pennsylvania, Philadelphia, Pennsylvania, 19104

Email: ivandmo@sas.upenn.edu

ABSTRACT

Supercharged proteins exhibit high solubility and other desirable properties, but no engineered superpositively charged enzymes have previously been made. Superpositively charged variants of proteins such as green fluorescent protein have been efficiently encapsulated within *Archaeoglobus fulgidus* thermophilic ferritin (AfFtn). Encapsulation by supramolecular ferritin can yield systems with a variety of sequestered cargo. To advance applications in enzymology and green chemistry, we sought a general method for supercharging an enzyme that retains activity and is compatible with AfFtn encapsulation. The zinc metalloenzyme human carbonic anhydrase II (hCAII) is an attractive encapsulation target based on its hydrolytic activity and physiologic

conversion of carbon dioxide to bicarbonate. A computationally designed variant of hCAII contains positively charged residues substituted at 19 sites on the protein's surface resulting in a shift of the putative net charge from -1 to +21. This designed hCAII(+21) exhibits encapsulation within AfFtn without the need for fusion partners or additional reagents. The hCAII(+21) variant retains similar esterase activity compared to wild-type, and spontaneously templates the assembly of AfFtn 24mers around itself. The AfFtn-hCAII(+21) host-guest complex exhibits both greater activity and thermal stability when compared to hCAII(+21). Upon immobilization on a solid support, AfFtn-hCAII(+21) retains enzymatic activity and exhibits an enhancement of activity at elevated temperatures.

Keywords:

carbonic anhydrase; host-guest complex; computational protein design; supercharged protein; templated self-assembly; enzyme immobilization

INTRODUCTION

Enzymes are increasingly employed in many green chemistry initiatives[1–9], particularly for chemical transformations that are difficult to achieve synthetically, often requiring low-yielding steps, expensive metal catalysts, and long workups in organic solvents. Living organisms have evolved systems of enzymes that carry out these reactions under mild aqueous conditions. Enzymes can be modified using directed evolution[5,10,11] or rational design[12–14] to enhance existing activities or gain new biosynthetic capabilities. The applications for engineered enzymes range from pharmaceuticals and organic transformations[15–17] to light harvesting and green feedstock generation[18]. Generally, enzymes are only marginally stable, and perform with optimal activity under very specific conditions. Beyond protein design and directed evolution, the stability and utility of these enzymes, such as increased tolerance to denaturing environments, can be increased through immobilization or encapsulation[19–22]. In employing these strategies, however, a decrement in enzyme activity often results when an enzyme is immobilized or modified[23], so it is useful to develop strategies for maintaining and protecting enzymatic activity.

Most proteins in nature have a low overall net charge, with a small subset being naturally supercharged[24]. These supercharged proteins serve functions in DNA condensation, fatty acid and protein synthesis, signal transduction, and antibacterial defense. While many naturally supercharged proteins are disordered, the small subset of folded supercharged proteins have inspired protein engineering efforts to redesign protein surfaces to display additional charged residues. Green fluorescent proteins (GFPs) were designed with theoretical surface charges ranging from -30 to +48, and these supercharged proteins gained thermal stability and a remarkable resistance to aggregation, as well as the ability to cross cell membranes[25,26]. Similarly, single-chain F_v antibodies against the bacteriophage MS2 have been supercharged from +5 to +20, giving them

greatly enhanced thermal stability and binding affinity[27]. Supercharged enzymes have also been designed; glutathione-S-transferase (GST)[25] and enteropeptidase[28] have been supernegatively charged (to -40 and -9, respectively), leading to increased solubility and thermal stability while still retaining enzymatic activity. Cellulases have been supercharged by multiple groups, ranging from -28 to +16[29,30], but none of the superpositively charged variants had their activity characterized. In other examples, the cellulase charge was engineered between -32.2 and +11.7[31], with the positive charge (+11.7) falling in the range of naturally occurring basic enzymes. More negatively supercharged enzymes may exist due to stabilization from surface-bound cations, and repulsion of anions that disrupt native hydrogen bonds[31,32]. Enzymes have also been genetically fused to supercharged GFPs for uses ranging from biomimetic packaging, cell delivery, and lipid nanoparticle formation[33–36]. However, to date, there are no examples to our knowledge of an engineered superpositively charged enzyme that goes beyond the limits of naturally occurring enzymes.

One goal of enzyme engineering is to leverage the unique catalytic capabilities of enzymes in new contexts and applications. For carbon capture and storage (CCS), nature has evolved highly efficient enzymes for the transport and conversion of carbon dioxide. Such enzymes are promising targets for exploring and engineering relevant features for CCS. Current industrial CCS processes include amine scrubbing[37], mineral carbonation into sedimentary basins and reactive rocks[38], capture by microalgae[39], and sequestration via adsorption onto a variety of materials[40–44], which require high pressure, large energy inputs, and/or the identification of specialized storage reservoirs. A potentially milder, more sustainable strategy involves leveraging nature's molecular machinery for carbon fixation, which begins with the chemical transformation of carbon dioxide.

Carbonic anhydrases (CAs) are a family of highly efficient enzymes that reversibly hydrate CO_2, generating HCO_3^-.

The well-studied isozyme, the 29 kDa human carbonic anhydrase II (hCAII) operates with near-diffusion-limited rates at ambient carbon dioxide pressures. Its active site contains Zn^{2+} coordinated in a distorted tetrahedral geometry with three histidine residues and a hydroxide ion or water molecule[45]. The enzyme is inexpensive to produce and purify in an active form using heterologous overexpression. In addition to its anhydrase activity, it can also act as an esterase, allowing for straightforward colorimetric detection of enzymatic activity. While hCAII has very fast kinetics ($k_{cat}^{CO2} \approx 10^6$ s^{-1}, $k_{cat}/K_m^{CO2} \approx 10^8$ M^{-1} s^{-1})[45], it is not well-suited for CCS at elevated temperatures (T > 50 °C). In addition, using hCAII in industrial applications requires enzyme immobilization, as free enzyme cannot be recycled from the reaction[46]. The efficiency of enzymes, including hCAII, is decreased upon immobilization via current methods involving adsorption[47], covalent crosslinking[48], entrapment[49,50] and encapsulation within a supramolecular host[51]. Using other robust proteins to protect or sequester enzymes provides a route to retaining enzyme activity in harsh environments, while facilitating immobilization or recovery of the associated enzymes.

Controlling the molecular features important for enzyme encapsulation and activity can be achieved within nanoscale supramolecular protein hosts. These host proteins range in size from 100-150 nm carboxysomes[52], to 20-250 nm viral capsids[53,54], ~30 nm lumazine synthase[35,55] and ~12 nm ferritin[56,57]. These protein hosts encapsulate a wide variety of cargo, including nucleic acids, nanoparticles and enzymes for use as nanoreactors[54,58,59], drug delivery vehicles[52–54,59–65], and bioimaging[66,67]. The three major methods for enzyme loading within these protein capsules rely on electrostatic interactions, affinity methods, or gene fusion[68]. Examples of loading using electrostatics include using nucleic acid tags on enzyme cascades inside cowpea chlorotic mottle

virus (CCMV)[69] and highly charged GFP(+36) inside lumazine synthase[70]. Affinity-based methods typically rely on insertion of tags and recognition sequences. One example includes making elastin-like polypeptide-CCMV fusions to encapsulate cargo with a C-terminal SrtA recognition site[71] while another utilizes a His tag and Ni^{2+} to form the assembly[72]. A SpyTag/SpyCatcher system was utilized to incorporate a two-enzyme indigo biosynthetic pathway within MS2-based capsids[73]. An α-helical sequence derived from the membrane plasma Ca^{2+} pump was inserted into the assembly domain of hepatitis B viral capsids to allow for Ca^{2+}-mediated assembly using cargo tagged with the C-terminal domain of calmodulin[74]. The addition of a C-terminal anchoring sequence allows cargo loading into encapsulins[75–78]. Many different cargoes have been investigated from a gene fusion standpoint, in which the cargo is fused directly to the protein cage monomers or other subunits. Bacteriophage P22 monomers have been fused with alcohol dehydrogenase D[58], CelB glycosidase[79], GFP and mCherry[80], and cytochrome P450[81], among other enzymes, and 13-MDa vault cages have been fused with luciferase and GFP[82]. Issues arise from the need for complicated fusions of enzymes with other proteins or increased steric hindrance within host proteins due to the additional components, so the use of a host-guest system that doesn't require additional proteins or protein domains is appealing.

Recent work from our lab and others has shown that thermophilic ferritin from *Archaeoglobus fulgidus* (AfFtn) can assemble around a superpositively charged protein, GFP(+36) as well as GFP(+36)-enzyme fusions[36,83], while high ionic strength is normally required for AfFtn assembly in the absence of a templating cargo. The AfFtn 24mer assembly is tetrahedrally symmetrical and has four large 4.5 nm triangular pores, allowing for more facile diffusion of substrate and products into and out of the cage[84]. While self-assembly of AfFtn around GFP(+36)-enzyme fusions has been reported, there are no examples of direct encapsulation of supercharged enzymes, which

allows the potential to fit more cargo inside the cage due to the absence of a 30 kDa fusion partner. Furthermore, this provides more opportunity for the enzyme itself to interact directly with the ferritin, instead of this interaction being mediated by the appended supercharged GFP. Previous studies from our laboratory showed that enzyme cargo can be loaded by using maleimide-mediated conjugation of superoxide dismutase to an engineered cysteine on the interior of AfFtn for use in targeted drug delivery[62]. We have also shown simpler methods of loading, as AfFtn can self-assemble around gold nanoparticles with complementary diameter and surface ligands, without requiring additional reagents[85–88]. One major advantage of encapsulation within AfFtn is that it can confer additional thermal stability to the cargo[36,89]. A general, one-step method for incorporating an enzyme within AfFtn would greatly expand the utility of this approach for enzyme immobilization. With thermally stable CAs from other organisms, encapsulation at room temperature results in only 60% retention of activity[51,90,91]. The highest activity upon encapsulation was a recent report showing 85% activity with a GFP(+36)-hCAII fusion[36]. Here, we explore the exciting potential to encapsulate hCAII in a stable ferritin protein scaffold, by engineering complementary surface charge interactions to favor encapsulation and robust enzyme activity.

We hypothesized that the surface of hCAII could be redesigned to give the enzyme a high overall net positive charge to promote encapsulation by AfFtn. This task is not straightforward, as many mutants have issues with expression, stability, and activity due to disruption of structure or from alterations to the catalytic mechanism. In a study where libraries of human 3-methyladenine DNA glycosylase (AAG) mutants were tested for viability, it was determined that the overall probability of inactivating AAG with a single random mutation is 34% [92]. Some smaller proteins appear to accept mutations more readily, as a random mutation in T4 lysozyme (164 residues) and barnase

(110 residues) led to inactivation at 16% and 5% of sites, respectively[93,94]. Nonetheless, the probability of inactivation of a protein is expected to increase with the increasing numbers of mutations.

An alternative to combinatorial methods is to use computational design to identify the positions on the hCAII surface that can be modified to positive charges. Computational design to modulate protein charge and electrostatic features has been established[27,29–31]. Herein, we applied a computational, probability-based design approach to redesign the enzyme[95–99]. Candidate exterior residues for mutation were selected by their solvent accessible surface areas (SASA)[100], and those mostly likely to support mutation to K and R were identified and used to guide the choice of mutations. In the resulting designed variant, twenty exterior residues were mutated from either a neutral or negatively charged amino acid to a positively charged amino acid. The putative net charge of each designed variant was quantified by simply neglecting variation of side-chain pK_a with location in the structure and summing amino acid ionization states expected at pH 7. The designed set of mutations increased the expected net charge of hCAII by +22 (in units of the electron charge), from a net charge of -1 for wild-type hCAII to +21 for the mutant. This designed construct hCAII(+21) was experimentally characterized for activity as well as for encapsulation within AfFtn, and the resulting AfFtn-hCAII(+21) complex was tested for activity at ambient and elevated temperature. Computational design of the superpositively charged enzyme enabled AfFtn encapsulation. Most promisingly, the resulting mutant maintained enzyme activity and gained thermal stability upon encapsulation within the ferritin host. The host-guest complex retained high enzymatic activity at elevated temperatures after immobilization on solid support.

MATERIALS AND EXPERIMENTAL DETAILS

Design of superpositively charged enzyme

To identify the exterior residues of hCAII to target for substitution, the solvent accessible area calculation tool GetArea[100] was applied to two crystal structures of human carbonic anhydrase II (PDB ID: 3KS3 and 3K34)[101] to determine the relative solvent accessible surface areas (SASA) of individual residues. Residues with a relative SASA greater than 40% in both structures were deemed to be exterior, yielding a set of 88 residues. G and P residues were excluded to minimize the perturbations to the correct folding of the protein, resulting in a list of 70 exterior residues. Among these exterior sites, 21 were positive residues (K or R) in the wild-type and eliminated, thus yielding a set of 49 candidate sites for amino acid variation. A probabilistic protein design method as described previously[95–97,102,103] was applied to the hCAII structure 3KS3. This probability-based design method has been applied previously to design variants of ferritin and ferritin-like proteins[96,97,103]. We note that others have also computationally design protein charge properties, often by applying a bias toward a particular charge state[27,29–31]. The calculations yield the probabilities of the allowed amino acids and their side chain conformations[104]. Computational studies were performed to identify where a C (cysteine) could be introduced to the surface of hCAII as a site for fluorophore attachment. This calculation was done allowing only wild type or C amino acids at each member of the set of 49 exterior residues, and residue 152 was chosen for the mutation S152C as it had the highest C probability. Subsequently, at each of the remaining 48 sites, wild type, K, R, and A were allowed. The remaining residues not targeted for mutation (interior residues and exterior G and P) were constrained to their wild-type crystallographic conformations, but the 21 exterior wild-type K and R residues were allowed to vary in their side chain conformations. The resulting probabilities of a positively charge amino acid (R or K) at each of the 48 residue sites were rank ordered. The top 20 mutations were used to specify hCAII(+23) and, after restoring wild type at D110, the remaining 19 mutations gave the +21

enzyme. The resulting sequence hCAII(+21) contains the following mutations: S152C, S73R, L57R, E187R, Q53R, T37R, L100R, S50K, T177R, S43R, E239R, S220K, Q158R, H36R, N253R, Q136K, S166K, Q74R, E14R, and L240R.

Primers used for mutagenesis of hCAII(+23) to hCAII(+21)

Forward: CCGAGCATACCGTGGATAAGAAAAAATACGCAG

Reverse: CTGCGTATTTTTTCTTATCCACGGTATGCTCGG

AfFtn protein expression and purification

AfFtn wt (UniProtKB O29424) was expressed and purified with slight modifications to previous publications[103]. Briefly, a plasmid containing AfFtn wt was transformed in BL21(DE3) cells (New England Biolabs). Cells were grown overnight at 37 °C in LB broth supplemented with 100 μg/mL ampicillin at 225 rpm. Cultures were transferred to 1 L Terrific Broth and grown at 37 °C supplemented with 100 μg/mL ampicillin at 225 rpm until OD_{600} ~0.8. Expression was induced with 1 mM IPTG for 4 h at 37 °C at 225 rpm. Cells were pelleted by centrifugation (10 min, 6 krpm, 4 °C) and stored at −20 °C. Cells were resuspended in buffer (20 mM sodium phosphate, 20 mM NaCl, pH 7.6) and lysed by treatment with lysozyme (~1 mg/mL final concentration), Benzonase® nuclease (Millipore Sigma) after addition of $MgCl_2$ to a final concentration of 2 mM, and sonication (amplitude of 30, 1 s on, 1 s off, 10 min total processing time). Cellular debris was removed by centrifugation (30 min, 13 krpm, 4 °C) and the soluble fraction was treated with Benzonase® nuclease for 30 min at rt after addition of $MgCl_2$ to a final concentration of 2 mM. The solution was heat shocked for 10 min at 80 °C to precipitate most *E. coli* proteins and centrifuged (9 krpm, 30 min, 4 °C). The supernatant was passed through a 0.22 μm filter and treated with Benzonase® nuclease for 60 min at rt after addition of $MgCl_2$ to a final concentration of 2 mM (so the AfFtn subunits were still dimers). The protein was concentrated and buffer

exchanged (20 mM sodium phosphate, 2.5 M NaCl, 2 mM EDTA, pH 7.6) with Amicon Ultra-15 centrifugal filters (MWCO = 30 kDa) and injected onto a HiLoad 16/60 Superdex 200 size exclusion column (GE Healthcare Life Sciences) equilibrated with high-salt buffer (20 mM sodium phosphate, 800 mM NaCl, pH 7.6). Fractions corresponding to 24mer (~60 mL elution volume) were collected and concentrated with Amicon Ultra-15 centrifugal filters (MWCO = 100 kDa), and were run through the size exclusion column two more times. Protein concentration was determined by the extinction coefficient at 280 nm calculated using ProtParam[105] (1.67 mL mg^{-1} cm^{-1}), and purity was confirmed using SDS-PAGE and A_{280}/A_{260} > 1.7. Expression and purification yielded ~50 mg protein/L of media. Protein solutions were stored at 4 °C until needed for experiments.

hCAII wt protein expression and purification

hCAII wt (UniProtKB P00918) was expressed and purified with slight modifications to our previous publication[106]. Briefly, a plasmid containing hCAII wt was transformed in BL21(DE3) cells. Cells were grown overnight at 37 °C in LB broth supplemented with 100 µg/mL ampicillin at 225 rpm. Cultures were transferred to 1 L LB supplemented with 100 µg/mL ampicillin at 225 rpm and grown at 37 °C until OD_{600} ~0.8. Expression was induced with 1 mM IPTG and 1 mM $ZnSO_4$ (final concentrations) overnight at 18 °C at 225 rpm. Cells were pelleted by centrifugation (10 min, 6 krpm, 4 °C) and stored at −20 °C. Cells were resuspended in phosphate-buffered saline (PBS) and lysed by treatment with lysozyme (~1 mg/mL final concentration), Benzonase® nuclease after addition of $MgCl_2$ to a final concentration of 2 mM, and sonication (amplitude of 20, 1 s on, 2 s off, 10 min total processing time). The lysate was clarified by centrifugation, and the supernatant was loaded onto a 5 mL HisTrap HP nickel immobilized-metal affinity chromatography column (GE Healthcare Life Sciences) in PBS. hCAII was washed with PBS

with 20 mM imidazole and eluted with PBS with 500 mM imidazole. Fractions containing hCAII were pooled, concentrated with an Amicon Ultra-15 centrifugal filter (MWCO = 10 kDa), and further purified by size exclusion chromatography using a HiLoad 16/600 Superdex 200 column. Fractions containing hCAII were pooled and concentrated using Amicon Ultra-4 centrifugal filters (MWCO = 10 kDa). Protein concentration was determined by the previously published extinction coefficient[83] at 280 nm (ε_{280} = 57,000 M^{-1} cm^{-1}) and purity was confirmed using SDS-PAGE. A280/260 > 1.7, expression and purification yielded ~25 mg protein/L of media. Protein solutions were stored at 4 °C until needed for experiments.

hCAII(+23/+21) protein expression and purification

hCAII(+23)-His_6 plasmid was purchased from ATUM, based on the computationally designed sequence and expressed based on previously published procedures[25,83], and hCAII(+23)-His_6 plasmid was obtained using PCR site-directed mutagenesis. The hCAII(+23/+21) plasmids were transformed in *E. coli* BL21(DE3) cells. Cells were grown at 37 °C overnight in LB broth supplemented with 50 µg/mL kanamycin at 225 rpm, transferred to 1 L LB supplemented with 50 µg/mL kanamycin, and grown at 37 °C at 225 rpm until OD_{600} ~0.8. Expression was induced with 1 mM IPTG and 1 mM $ZnSO_4$ (final concentrations) overnight at 18 °C at 225 rpm. Cells were harvested by centrifugation and stored at −20 °C. Cells were resuspended in lysis buffer (PBS with 2 M NaCl) and lysed by treatment with lysozyme (~1 mg/mL final concentration), Benzonase® nuclease after addition of $MgCl_2$ to a final concentration of 2 mM, and sonication (amplitude of 20, 1 s on, 2 s off, 10 min total processing time). The lysate was clarified by centrifugation (13 krpm for 30 min). Initial purification was performed using HisPur™ Ni-NTA spin columns (Thermo Fisher), washing three times with lysis buffer containing 20 mM imidazole and 10% glycerol, followed by elution with lysis buffer containing 500 mM imidazole and 10% glycerol.

Elution fractions were collected and buffer exchanged to PBS with 10% glycerol. Benzonase® nuclease and $MgCl_2$ (2 mM final concentration) were added and the solution was incubated at rt for 60 min to further remove nucleic acids. Using a HiTrap SP HP column (GE Healthcare Life Sciences), cation exchange was performed by running a gradient 0–100% lysis buffer over 25 mL using PBS and lysis buffer. The sample was then concentrated using Amicon Ultra-15 centrifugal filter (MWCO = 10 kDa), and further purified by size exclusion chromatography in PBS using a HiLoad 16/600 Superdex 200 column. Fractions from the peak showing qualitative ability to convert 4-nitrophenyl acetate (pNPA) to 4-nitrophenol (pNP) (yellow color change) were pooled and concentrated using Amicon Ultra-4 centrifugal filters (MWCO = 10 kDa). Purity was verified by SDS-PAGE (Fig. S14) and concentration was determined using the extinction coefficient at 280 nm calculated using ProtParam (ε_{280} = 50,500 M^{-1} cm^{-1}). This process yielded titers around 25 mg of enzyme per L of culture. Protein solutions were stored at 4 °C until needed for further experiments. hCAII(+21) samples from which nucleic acids were rigorously removed during purification gave a ratio of absorbances at 280 nm (A_{280}) and 260 nm (A_{260}) of $A_{280}/A_{260} > 1.7$. Expression and purification yielded ~15 mg protein/L of media.

hCAII(+21) Non-Native Surface Cys152 Dye Labeling

From the purified protein stock, a 500 µL solution of 100 µM hCAII(+21) was prepared with 5 mM TCEP in an opaque Eppendorf tube and incubated for 1 h at 4 °C to ensure that the protein was fully reduced. Following the incubation, freshly dissolved Oregon Green Maleimide (Thermo Fisher) in DMSO was added dropwise to the hCAII(+21) protein incorporating C152. Final concentrations gave dye in 20-fold excess. The reaction proceeded overnight at 4 °C. The reaction was then purified by PD-10 desalting column (GE Healthcare Life Sciences) and the resulting

fractions were analyzed by UV-Vis spectroscopy. The dye-labeled protein fractions were pooled and concentrated using Amicon Ultra-0.5 centrifugal filters (MWCO = 10 kDa).

Determination of hCAII(+21) Labeling

The measured A_{280} of dye-labeled hCAII(+21) has contributions from both hCAII(+21) and Oregon Green, while A_{492} is only due to Oregon Green. The concentration of Oregon Green was determined using the manufacturer's extinction coefficient (ε_{492} = 87,000 M^{-1} cm^{-1}). The ratio of A_{280}/A_{492} for Oregon Green Maleimide was experimentally determined to be 0.145. This was used to calculate the A_{280} that can be attributed to hCAII(+21) in the dye-labeled hCAII(+21). The concentration of hCAII(+21) was determined using the extinction coefficient previously described, correcting for the absorbance due to Oregon Green, yielding the labeling percentage or [Oregon Green]/[hCAII(+21)] = 56%.

$$Labeling\ \% = \frac{[Oregon\ Green]}{[hCAII(+21)]} = \frac{\frac{A_{492}}{\varepsilon_{492\ Oregon\ Green}}}{\frac{A_{280} - (A_{492} \times 0.145)}{\varepsilon_{492\ hCAII(+21)}}} = 56\%$$

AfFtn-hCAII(+21) Complex Formation

AfFtn–hCAII(+21) complexes were formed by mixing hCAII(+21) and AfFtn dimer in a 1:12 or 1:6 ratio in no-salt buffer (20 mM sodium phosphate, pH 7.6) at a concentration of 0.6 μM for native agarose gel electrophoresis, 1.0 μM for pNPA assay and 6.0 μM for size exclusion chromatography (based on AfFtn 24mer), equilibrating overnight at 4 °C. AfFtn-hCAII(+21) samples used in the Ni-NTA assays, Centricon MWCO assays, and activity assays were isolated 24mer peaks after further SEC purification.

Native Gel Electrophoresis

Native gels (0.7% agarose) were prepared in 5 mM NaCl, 20 mM sodium phosphate, and pH 7.6. Samples were mixed with glycerol (final concentration 16% v/v) immediately prior to running. Gels were run at 100 V for 20 min on ice. Gels were imaged using a Typhoon FLA7000 imager using an excitation wavelength of 472 nm and PMT setting of 500 V. Following fluorescence imaging, gels were stained with Coomassie Brilliant Blue R-250.

Size Exclusion Chromatography

Analytical SEC was performed with an AKTA Pure FPLC system using a Superdex200 Increase 10/300 GL column equilibrated with no-salt buffer (20 mM sodium phosphate, pH 7.6). Samples were prepared as indicated above. Sample (200 µL) was injected and A_{280} and A_{492} were monitored. The sample was eluted at rt using a flow rate of 1.0 mL/min.

Dynamic Light Scattering

Sample (100 µL) was pipetted into a disposable micro cuvette (BrandTech Scientific). DLS was performed on a Malvern ZetaSizer Nano ZS with a scattering angle of 173° at 25 °C (1 min equilibration time).

Fluorescence measurements

Fluorescence analysis of Ni-NTA assay and Centricon MWCO assay samples was performed with a Tecan M1000 microplate reader. Sample (100 µL) was pipetted into a black 96-well plate (Greiner Bio-One). Oregon Green-labeled protein samples were excited at 492 nm and fluorescence was measured at 516 nm.

Ni-NTA Assay

AfFtn-hCAII(+21) samples (100 µL) were prepared as described above and mixed with 100 µL of Ni-NTA resin that had been pre-washed with no-salt buffer (20 mM sodium phosphate, pH 7.6). Samples were incubated for 1 h at 4 °C on an end-over rocker, covered in foil. Post-incubation,

samples were centrifuged for 1 min at 13 krpm to pellet the resin. The supernatant was moved to a clean tube for later analysis ("load"). The resin was resuspended in lysis buffer containing 20 mM imidazole, centrifuged, and again the supernatant was removed ("wash 1"). This was repeated twice more ("wash 2," "wash 3"). After washing, the resin was resuspended in lysis buffer containing 500 mM imidazole, centrifuged, and the supernatant was removed ("elution 1"). Again, this was repeated twice more ("elution 2," "elution 3"). The fluorescence of all supernatant samples was measured using a microplate reader as described above.

Centricon MWCO Assay

AfFtn-hCAII(+21) samples (500 µL) were prepared as described above and spun in Amicon Ultra-0.5 centrifugal filter (MWCO = 10 kDa) for 15 min at 13 krpm. The fluorescence of the flowthrough and the retained volume were each measured using the microplate reader.

Determination of hCAII(+21) Loading

AfFtn-hCAII(+21) samples were analyzed by SEC and the A_{280} and A_{492} values were used to calculate the number of hCAII(+21) proteins per AfFtn 24mer. The concentration of AfFtn was calculated using $A_{280,AfFtn}$ and the extinction coefficient above, correcting for the relative absorbance of dye-labeled hCAII(+21) at 280 nm using its absorbance at 492 nm while the concentration of hCAII(+21) was calculated based on A_{492} and dividing by the labeling percentage. The loading, [hCAII(+21)] / [AfFtn 24mer], was then calculated.

$$Loading = \frac{[hCAII(+21)]}{[AfFtn\ 24mer]} = \frac{\frac{A_{492}}{\varepsilon_{492\ Oregon\ Green} \times 56\%\ loading}}{\frac{A_{280} - (A_{492} \times 0.658)}{\varepsilon_{280\ hCAII(+21)}}}$$

pNPA Assay

pNPA assays were performed in a Multizone CARY 3500 UV-Vis spectrometer with slight modifications to published procedures[107]. Samples (270 μL) were prepared at an enzyme concentration of 1 μM. Inhibition assays were performed with 10 μM acetazolamide. Samples were then pipetted into 1 mL quartz cuvettes (Starna Cells, Inc.) and brought to temperature in the UV-Vis instrument as measured by the in-cuvette temperature probes. pNPA (30 μL at 10 mM) was added to the cuvette and the solution was pipetted up and down 7 times to mix (0.9 μM enzyme, 1 mM pNPA). A_{410} was measured every 10 s for 2 min to monitor the evolution of pNP, and the rate was calculated from the linear rate determined between 30 s and 60 s, with one unit being defined as the mg amount of enzyme that releases 1 μmol of pNP per min[46,108].

Enzyme immobilization on agarose resin

hCAII wt, hCAII(+21), and AfFtn-hCAII(+21) were covalently immobilized to 33 mg Pierce NHS-Activated Agarose Spin Columns (Thermo Fisher) according to manufacturer recommendations. Briefly, 400 μL samples of 0.5 or 1.0 μM enzyme/complex in PBS were incubated with dry resin mixing end-over-end for 2 h at rt then overnight at 4 °C. The solution was spun down and coupling efficiency was measured based on the Bio-Rad Protein Assay (Bio-Rad) (hCAII wt and hCAII(+21) >99%, AfFtn-hCAII(+21) 50-80%). The resin was washed at least twice with PBS and remaining resin active sites were blocked by incubating with 400 μL quenching buffer (1 M tris pH 7.4) for 20 minutes at rt with end-over-end mixing. The resin was washed at least thrice with PBS and resin with immobilized enzyme was ready to use in subsequent studies.

pNPA Assay of immobilized enzyme

Immobilized enzyme samples were prepared as described above. PBS (270 μL) was added to each spin column then pNPA (30 μL at 10 mM in ACN) was added and the solution was pipetted

up and down 7 times to mix. Columns were rotated end-over-end at rt or 60 °C for 60 s then the solution was spun through. Flowthrough A_{410} was measured via UV-Vis to monitor the evolution of pNP, then the resin was washed with at least thrice with PBS until one wash after all yellow color was gone. Resin was then used for two more subsequent pNPA assays. All values were corrected against resin-only samples.

CD Tm Determination

10 μM samples of hCAII wt and hCAII(+21) (300 μL) were prepared in no-salt buffer and pipetted into 1 mm quartz cuvettes (Hellma USA). Samples were run in a JASCO J-1500 circular dichroism spectrometer and heated at a rate of 12 °C/h from 10 °C to 90 °C, monitoring θ_{205} (hCAII). The melting temperature, T_m, was determined by finding the temperature at which 50% of starting ellipticity was lost. Thermal melt shown as fraction folded, comparing θ and θ_{max} as described below.

$$Fraction\ Folded = 1 - \frac{\theta_{max} - \theta}{\theta_{max}}$$

RESULTS AND DISCUSSION

Design of superpositively charged enzyme

A high resolution structure of hCAII (PDB ID: 3KS3)[109] was chosen as the template structure for computational design. Exterior residues were identified as those having greater than 40% solvent accessible surface area (SASA),[100] and those whose wild-type identities were G, P, K or R residues not considered for mutation; this yielded a set of 49 exterior residues (and no active site residues) as potential sites for redesign. The design calculations apply a computational method that yields the probabilities of amino acids at variable positions in a given protein structure[95–97,102,103]. Computational studies were performed to identify where a C (cysteine) could be introduced to the surface of hCAII as a site for fluorophore attachment. This initial calculation

allowed only wild type or C amino acids at each of the selected exterior residues, and residue 152 was chosen for the mutation S152C as it had the highest C probability. To identify exterior positions suitable for positive charges, calculations were carried out for the remaining 48 exterior residues (152 was kept as C), where the wild-type amino acid, K, R and A were allowed at each variable residue position and all positions were allowed to vary in the calculation. The inclusion of A was used to accommodate mutation from wild type to a smaller amino acid if required to accommodate mutations to K or R elsewhere in the structure. The sum of the probabilities of K and R, $p_+ = p(K) + p(R)$, was used to quantify a site's propensity for presenting a positively charged amino acid. The 48 candidate sites were ranked by their p_+ probability values. The top 20 residues exhibited $p_+ > 0.4$, and if all 20 were mutated they would yield a variant with a +23 overall net charge (Figure S1). The backbone dihedral angles (ϕ,ψ) were examined using the usual Ramachandran plot (Figure S2). D110 in the crystallographic structure occupies the left-handed alpha-helical region (near $\phi = \psi = +60°$), which is known from database studies to be mainly populated predominantly by only G, N, and D residues[110]. Residue 110 is within a loop in hCAII, and mutation at this site has the potential to disrupt the stability of the enzyme. Designed variants with (D110K) and without (D110) the mutation and having charges of +23 and +21, respectively, were both advanced for experimental studies. We denote these two constructs by their expected charges: hCAII(+23) and hCAII(+21).

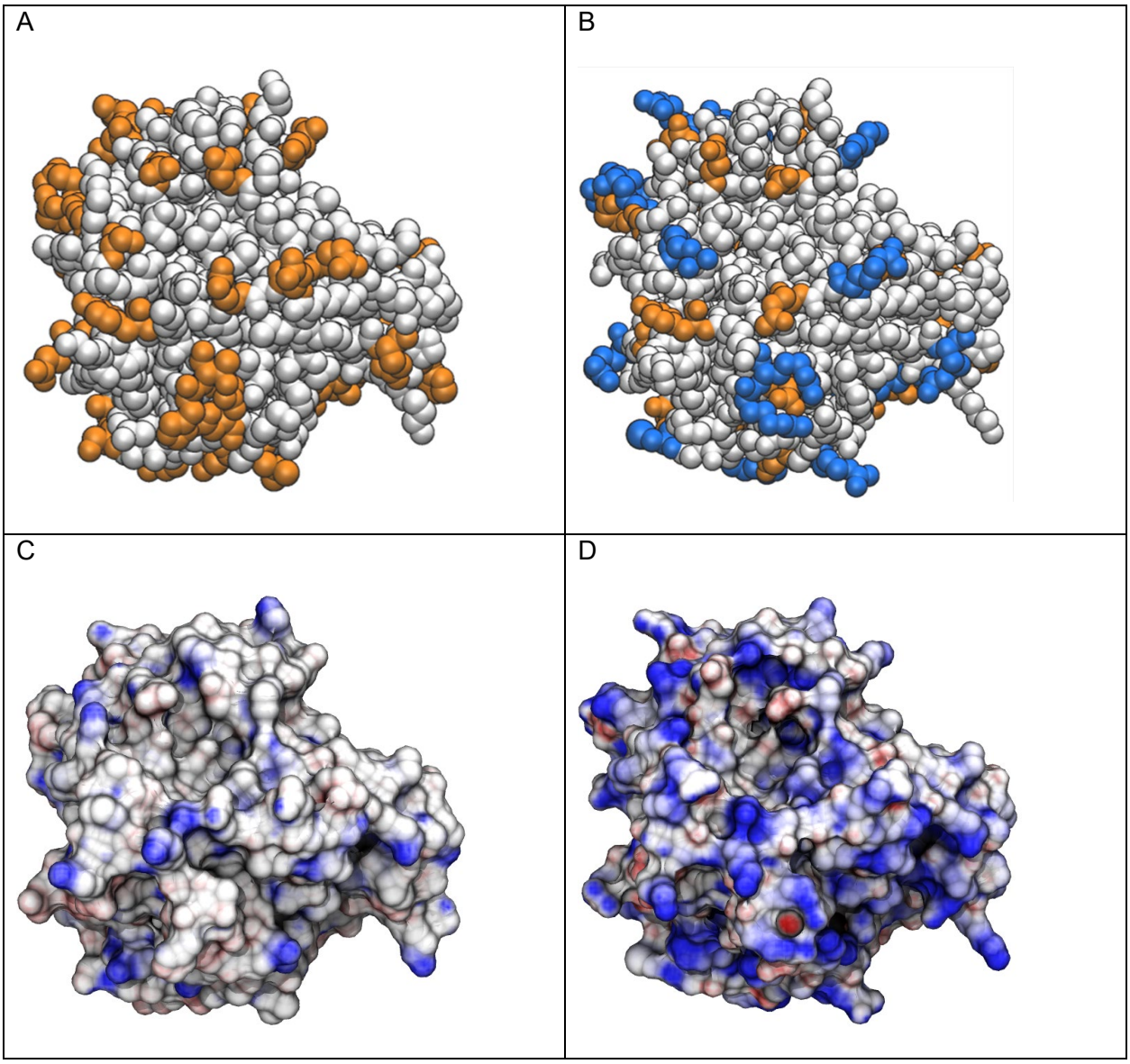

Figure 1. (A) Rendering of wild type hCAII. Residues selected for redesign (49 exterior residues) are colored in orange. (B) Rendering of hCAII(+21). Unchanged exterior residues considered for substitution are colored in orange. Twenty mutated residues (including S152C) are colored in blue. (C) Electrostatic surface of wildtype hCAII. (D) Electrostatic surface hCAII(+21). Electrostatic

surface renderings are colored to indicate expected charge from negative (red) to positive (blue) and rendered using the APBS plugin[111] of VMD[112].

The plasmid for hCAII(+23) with a C-terminal hexahistidine tag was ordered (Atum Bio), site-directed mutagenesis was performed to make the plasmid for hCAII(+21). Both proteins were expressed in *E. coli*. A large population of the expressed hCAII(+23) protein ended up forming inclusion bodies (Figure S3) that did not refold upon snap dilution after pre-extraction with urea and Triton X-100 and solubilization with 8 M guanidine HCl and dithiothreitol (DTT). The small portion of expressed hCAII(+23) that remained soluble purified as inactive, soluble aggregates, eluting in the void volume of the size exclusion column during size exclusion chromatography (SEC) (Figure S4). In contrast, hCAII(+21) expressed as a soluble, monomeric, active protein and eluted during SEC with the expected retention time for a 29 kDa protein (Figure S5). The surface mutations of hCAII(+21) led to a slight loss of thermal stability and reduction in the folding temperature (T_m = 55 °C → 51 °C) relative to wild type as shown by thermal melts monitored by circular dichroism (CD) (Figure S6). The large number of mutations of like charge may reduce stability and structural integrity of the enzyme to a degree. As a result of these findings, hCAII(+21) was chosen as the supercharged enzyme variant for further study (Figure 1, Figure S7).

We found that the esterase activity of hCAII(+21) is 81% of that of hCAII wt (Figure 2), where activity is monitored via the conversion of 4-nitrophenyl acetate (pNPA) to 4-nitrophenol (pNP) at rt,. To confirm that esterase activity is due to hCAII(+21), the pNPA assay was also performed with 10 μM acetazolamide, a widely used non-competitive inhibitor of CAs. The sample with both protein and inhibitor exhibited the same low activity as inhibitor alone,

suggesting that turnover occurs at the active site of the enzyme (Figure S8). No pNP formation was observed in the presence of only AfFtn; this ferritin does not catalyze the hydrolysis.

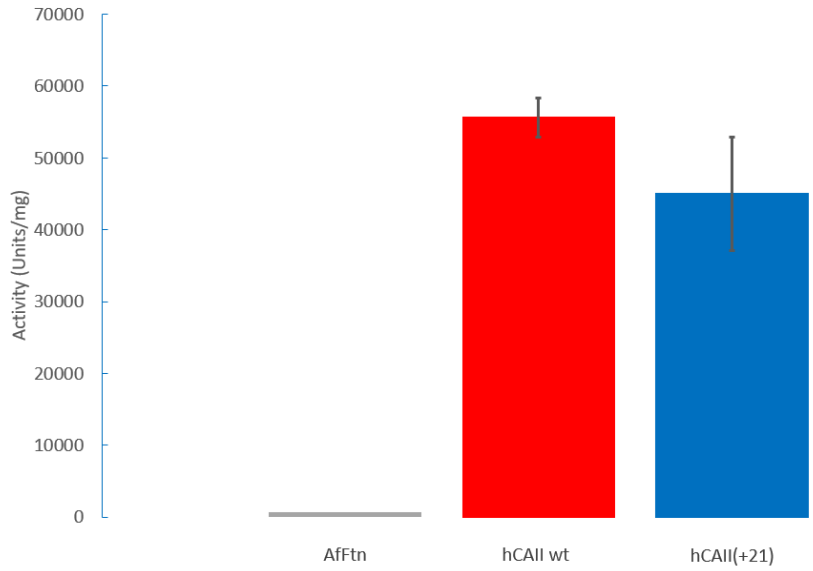

Figure 2. pNPA assay of AfFtn, hCAII wt and hCAII(+21). pNPA activity assay of AfFtn, hCAII wt and hCAII(+21) at rt show that expressed hCAII(+21) is an active enzyme that is able to hydrolyze pNPA to pNP at 81% of the rate of hCAII wt, while AfFtn does not hydrolyze pNPA. Error bars indicate the standard error of triplicate measurements.

Superpositively charged enzyme is encapsulated by AfFtn

hCAII (wt or hCAII(+21)) and AfFtn (as dimers of four-helix bundles) were mixed in 1:12 stoichiometry in a low ionic strength buffer ("no-salt" buffer, meaning no added NaCl, 20 mM sodium phosphate, pH 7.6) to maintain AfFtn as dimers prior to mixing. The solutions were assessed by size-exclusion chromatography (SEC). AfFtn and hCAII wt did not interact, as shown by the elution of an AfFtn dimer peak at 17 mL and a free hCAII wt peak at 23 mL (Figure S9). In contrast, hCAII(+21) induced formation of AfFtn 24mer. We fluorescently labeled hCAII(+21)

to monitor the encapsulation. Oregon Green-labeled hCAII(+21) induced AfFtn 24mer assembly and encapsulation, as indicated by an elution peak (both A_{280} and A_{492}) at 13 mL, the normal elution volume of ferritin 24mer on the Superdex200 Increase column. Monitoring A_{280} and A_{492} during SEC of Oregon Green-labeled hCAII(+21)-AfFtn (Figure 3), we were able to determine that the average number of hCAII(+21) molecules per AfFtn 24mer was 1.6 ± 0.1, suggesting a range of 1-to-2 hCAII(+21) molecules encapsulated per AfFtn 24mer. This loading ratio is smaller than prior studies with GFP(+36)-AfFtn (2.5:1)[83] and is also smaller than the ratio observed with most other cargo in much larger protein cages (2-96:1)[55,59,71,73,77,82,113]. The sample homogeneity and nearly 1:1 stoichiometery of hCAII(+21)-AfFtn facilitates biophysical measurements and enzyme studies.

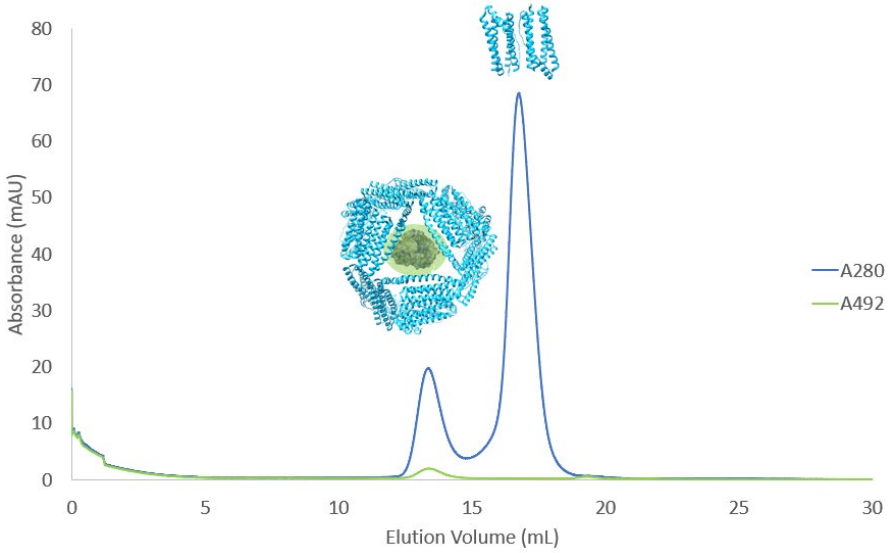

Figure 3. SEC of the 1:1 AfFtn-hCAII(+21) complex in no-salt buffer. The peak at 13 mL (A_{280} and A_{492}) corresponds to the formation of AfFtn 24mer. A_{492} peak from the Oregon Green-labeled hCAII(+21) confirms that hCAII(+21) is encapsulated by AfFtn.

The 24mer AfFtn-hCAII(+21) sample was then measured by dynamic light scattering (DLS), yielding an average diameter of 14.5 nm (PDI = 0.06), which is similar to the previously published 13.9 nm diameter for empty AfFtn 24mer[103] in high-salt buffer. This indicated that hCAII(+21) was successfully encapsulated and not simply adsorbed to the surface or contained in non-specific aggregates (Figure S10).

Samples of Oregon Green-labeled hCAII(+21) and AfFtn were prepared and run on a 0.7% agarose gel under low-salt conditions (5 mM NaCl, 20 mM sodium phosphate, pH 7.6) (Figure 4). Gel fluorescence imaging shows that hCAII(+21) on its own stays in the loading well, which is expected given the polarity of the applied voltage and the large positive charge of the protein. In the presence of AfFtn, hCAII(+21) migrates with the AfFtn 24mer band further down the gel than AfFtn dimer. The Coomassie-stained image of the same gel corroborates these findings, as samples containing both AfFtn and hCAII(+21) migrate furthest towards the positive terminal.

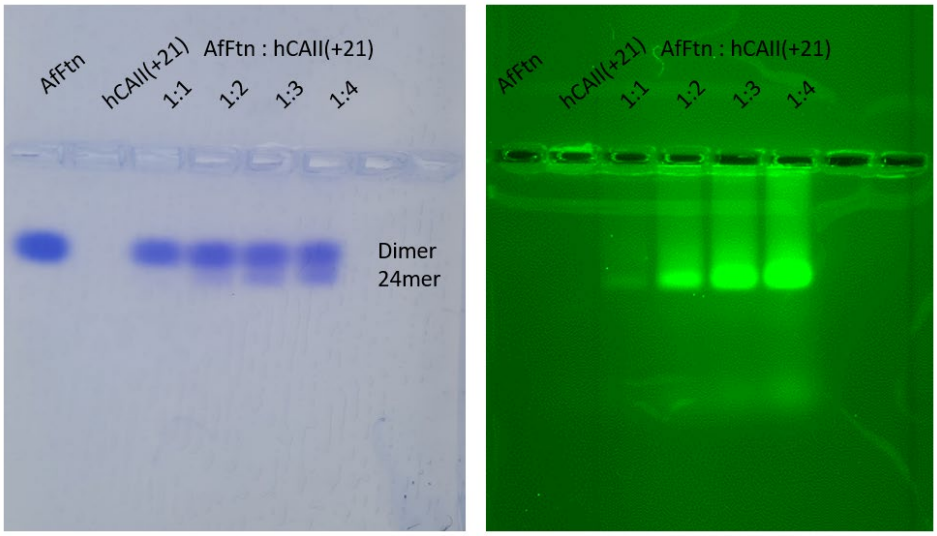

Figure 4. Native agarose gel of AfFtn and hCAII(+21). Native agarose gel electrophoresis of AfFtn 24mer:Oregon Green-labeled hCAII(+21), stained with Coomassie blue (left) and fluorescently imaged (right). AfFtn (dimer) alone runs towards the positive terminal and in the

presence of excess hCAII(+21) the emergence of a second (24mer) band can be seen. Alone, hCAII(+21) stays in the loading well but in the presence of AfFtn, the complex runs towards the positive terminal.

To further confirm encapsulation of hCAII(+21), we incubated Oregon Green-labeled hCAII(+21) and Oregon Green-labeled hCAII(+21)-AfFtn samples with nickel nitrilotriacetic acid (Ni-NTA) agarose resin (Figure 5). Only hCAII(+21) should bind the Ni-NTA resin due to its His_6 tag. When hCAII(+21) was incubated with the resin alone, most of the fluorescence was seen in fractions after exposure to 500 mM imidazole (elution), confirming that hCAII(+21) binds the resin. For the AfFtn-hCAII(+21) sample, most of the fluorescence was observed in the flowthrough and wash fractions, indicating that hCAII(+21) was encapsulated inside AfFtn, where the His_6 tag interacted minimally with the beads.

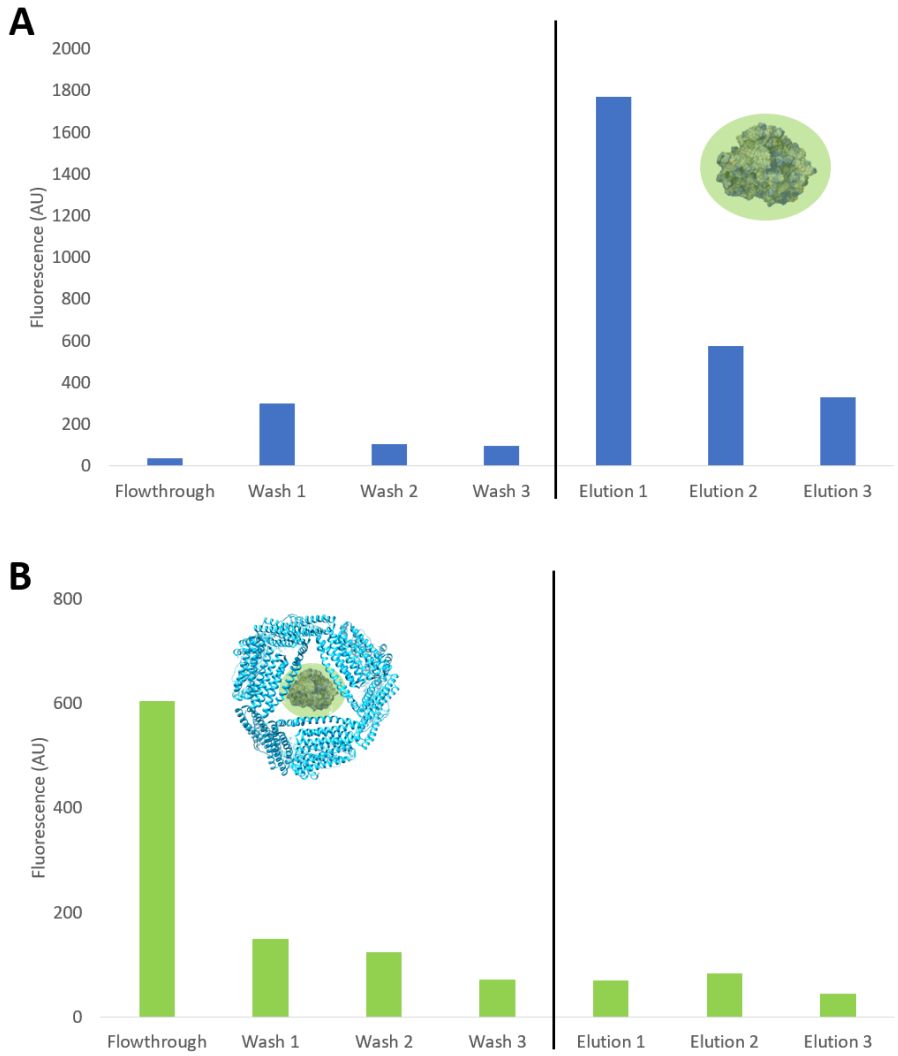

Figure 5. Ni-NTA binding assay of hCAII(+21) (A) and the AfFtn-hCAII(+21) complex (B). By itself, hCAII(+21) binds the Ni-NTA resin and very little fluorescence is seen in the load and wash (20 mM imidazole) fractions (A). When eluted with 500 mM imidazole, greater fluorescence is seen in the elution fractions. For the AfFtn-hCAII(+21) sample (B), most of the fluorescence is seen in the load and wash fractions.

Another method testing encapsulation was a molecular weight cutoff (MWCO) filter-based assay using Centricon tubes (Figure 6). Based on the 100 kDa MWCO of the Centricon tube, AfFtn dimer and unencapsulated hCAII(+21) should flow through the membrane after spinning,

while the AfFtn-hCAII(+21) sample should be retained. In the hCAII(+21) control, a majority of the fluorescence was indeed seen in the flowthrough, confirming that hCAII(+21) passes through the 100 kDa MWCO filter membrane. The AfFtn-hCAII(+21) sample showed almost all of the fluorescence in the retained volume and comparatively little fluorescence in the flowthrough, further confirming that hCAII(+21) was encapsulated.

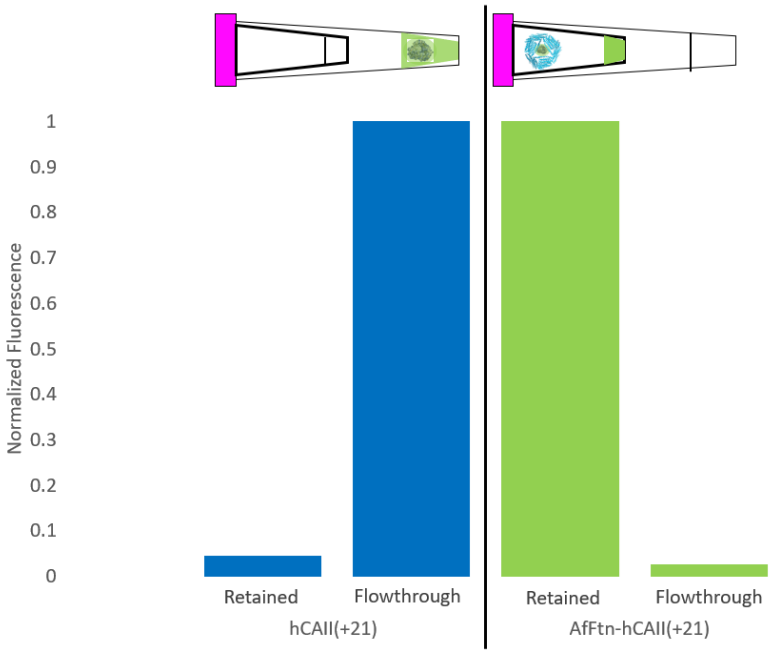

Figure 6. Centricon Assay of AfFtn and hCAII(+21). MWCO based Centricon Spin Filtration Assay of hCAII(+21) and the AfFtn-hCAII(+21) complex. Alone, the ~30 kDa hCAII(+21) sample easily passes through the 100 kDa MWCO filter membrane and a majority of the fluorescence is seen in the flowthrough. For the AfFtn-hCAII(+21) sample, the ~500 kDa AfFtn 24mer is too large to pass through the 100 kDa MWCO filter membrane and most of the fluorescence is seen in the retained volume, agreeing with the results of the Ni-NTA assay.

Superpositively charged enzyme retains high activity within AfFtn

Having established that engineered hCAII(+21) is an active enzyme that can be encapsulated by AfFtn, we tested the enzyme activity of encapsulated hCAII(+21) (Figure 7). At 30 °C, hCAII(+21) has 88% of the activity of hCAII wt. More strikingly, upon encapsulation within AfFtn, 97% of hCAII(+21) activity was retained relative to non-encapsulated hCAII(+21). This is the most efficient encapsulated CA system to date, compared with 85% retention of activity after encapsulation of a GFP-enzyme fusion and only 60% retention of activity shown in prior protein host-guest examples[47–49]. Upon increasing the temperature to 40 °C, hCAII wt activity increased by 40% while hCAII(+21) decreased in activity by 32%. AfFtn-encapsulated hCAII(+21) showed 63% enhanced activity at 40 °C relative to free hCAII(+21). At 50 °C and 60 °C both enzymes lost most of their activity.

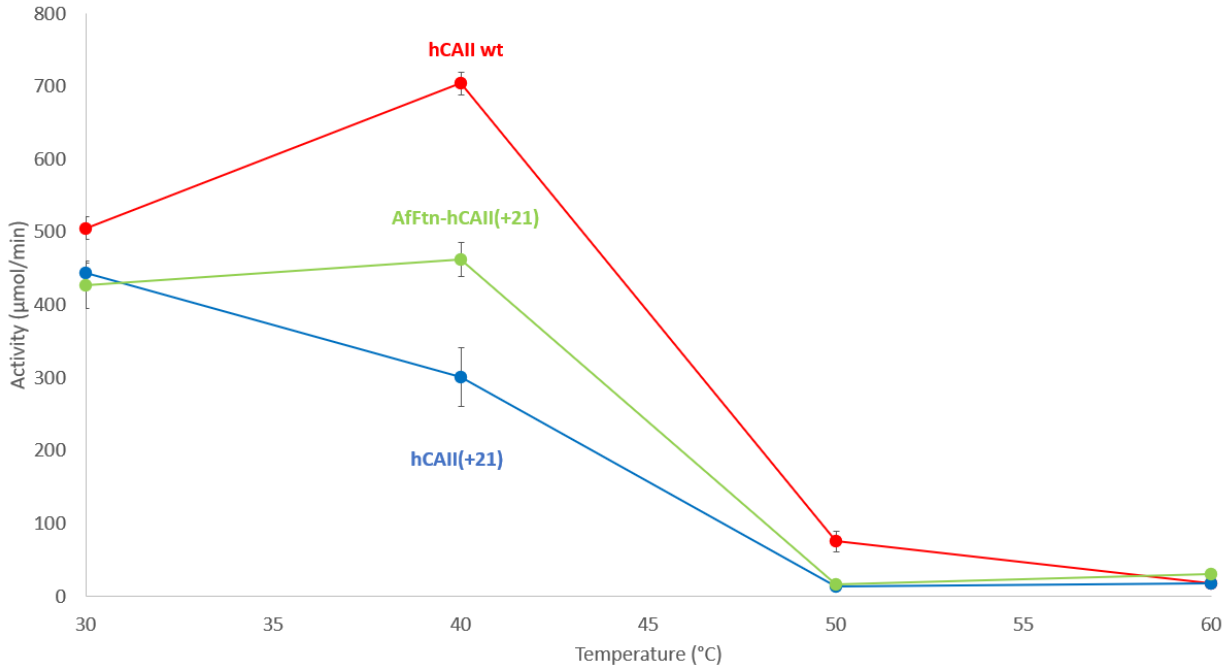

Figure 7. pNPA activity assay of 1 µM enzymes from 30 °C to 60 °C. While both hCAII wt and hCAII(+21) experience a large decrement in activity at 50 °C, encapsulating hCAII(+21) within AfFtn preserves activity at 40 °C. Error bars indicate the standard error of triplicate measurements.

Host-guest complex exhibits high activity at elevated temperatures after immobilization to solid support

One of the biggest challenges in surface enzyme immobilization is the loss of activity that many enzymes experience upon immobilization. NHS-agarose activated resin was selected due to the ease of reacting NHS groups with primary amines on the enzyme surface and the stability and hydrophilicity of the agarose[114]. hCAII wt and hCAII(+21) were loaded with close to 100% efficiency while AfFtn and the AfFtn-hCAII(+21) complex were loaded with 50-80% efficiency. Although the activity of the enzymes decreased upon immobilization at rt, they remained highly active towards pNPA, while AfFtn showed no activity (Figure 8). Immobilization to the resin provided considerable thermal stability to both hCAII wt and hCAII(+21), which had comparable activity at 60 °C vs rt. Activity of the AfFtn-hCAII(+21) complex nearly tripled at the elevated temperature. One possible explanation for this phenomenon is that the AfFtn adopts a more compact structure upon immobilization and forms more contacts with hCAII(+21), similar to how enzymes loaded into size-matched metal-organic frameworks (MOFs) exhibit enhanced stability and activity[20,115]. Enzyme immobilization often results in an expansion of the temperatures where the enzyme is active and can also shift the maximum activity towards higher temperatures[47,49,116–118]. Importantly, the ferritin-encapsulated and immobilized enzyme is also reusable, retaining activity after multiple runs. This demonstrates the versatility of immobilizing enzyme-loaded AfFtn and could be generalizable to other types of solid supports.

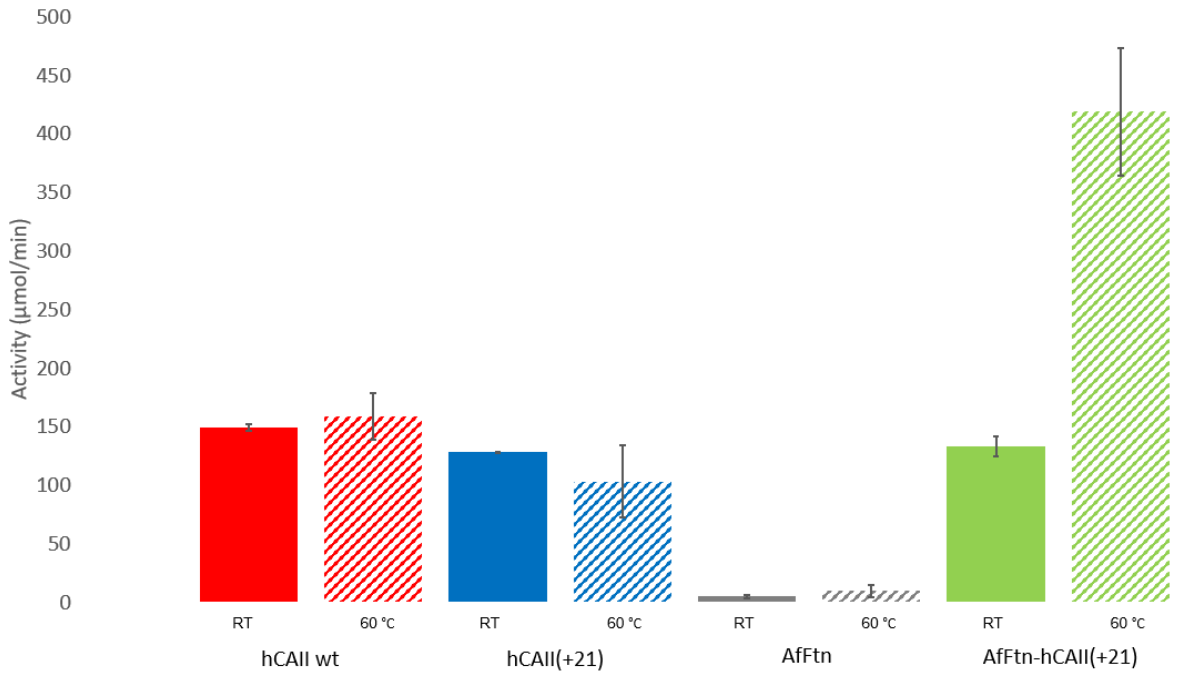

Figure 8. pNPA activity assay of immobilized enzymes at rt and 60 °C. Immobilized enzymes lose activity upon immobilization relative to free enzyme in solution, but activity is little affected when raising the reaction temperature to 60 °C except for the AfFtn-hCAII(+21) complex, which experiences a threefold increase. Immobilized AfFtn shows negligible activity at both temperatures. Error bars indicate the standard error of triplicate measurements, in which enzymes were reused for subsequent runs.

CONCLUSIONS

In conclusion, we have engineered the surface of hCAII to display a theoretical overall charge of +21 to give it the ability to template the formation of AfFtn 24mers around it while maintaining enzyme activity. Methods of characterizing hCAII(+21) by SEC, DLS, SDS-PAGE, CD thermal melts and esterase assays confirm the identity and activity of the enzyme. SEC, Ni-NTA and Centricon MWCO assays, and native agarose gels verify that hCAII(+21) is encapsulated

within AfFtn cages. hCAII(+21) retains high activity even upon encapsulation and immobilization and gains thermal stability within the AfFtn cavity, especially after immobilization.

We provide the first example of a designed superpositively charged enzyme, which is able to induce AfFtn 24mer assembly without the need for salt or a superpositively charged fusion partner. This provides a general strategy for redesigning the surface of an enzyme for encapsulation within the thermally stable AfFtn protein host. Having immobilized a superpositively charged enzyme within AfFtn and the resulting host-guest complex on solid support and observing both the retention of high enzymatic activity and thermal stabilizing effects, AfFtn emerges as an even more intriguing protein host. Strategies for maximizing enzyme activity in scenarios relevant to carbon dioxide sequestration still remain to be explored. Additionally, due to sample homogeneity and the low guest:host ratio, these complexes are attractive candidates for further characterization, e.g., to elucidate the charge complementarity at the AfFtn-enzyme interface, its role in 24mer assembly, and effects associated with immobilization. Overall, this approach can be employed with a variety of other enzymes that could benefit from the protection of a thermophilic protein cage for applications in green chemistry and therapeutic enzyme delivery.

ASSOCIATED CONTENT

Supporting Information Available: The following files are available free of charge. Biochemistry_SI.pdf

- Exterior residues K+R probability ranking, Ramachandran plot of exterior residues, SDS-PAGE and SEC of hCAII(+23) overexpression, SDS-PAGE of hCAII(+21), CD thermal melts, sequence alignment, DLS, and plasmid info of hCAII wt and hCAII(+21), acetazolamide inhibition of hCAII(+21), SEC of AfFtn-hCAII(+21).

Accession Numbers

Sequences for hCAII(+23) (GenBank Accession No. MW770314) and hCAII(+21) (GenBank Accession No. MW770315) have been deposited in the GenBank Data Libraries.

Author Contributions

J.A.B. expressed, purified, and characterized all proteins, and performed all encapsulation and enzyme activity assays. R.G. performed all computational design. Z.W. and M.A.D. helped with protein expression and purification. I.J.D. and J.G.S. oversaw the project and provided guidance. All authors edited the manuscript and have given approval to the final version of the manuscript.

Funding Sources

Funding for this work was provided by the NSF (CHE-1905203) to IJD and JGS, the Vagelos Institute for Energy Science and Technology (graduate fellowship) to JAB, and the LRSM MRSEC IRG-3 (NSF DMR-1720530) to IJD. Protein modelling and design employed the Extreme Science and Engineering Discovery Environment (XSEDE), which is supported by NSF grant no. ACI-1053575, under grant no. TG-CHE110041.

Notes

The authors declare no competing financial interest.

ACKNOWLEDGEMENTS

ABBREVIATIONS

AfFtn: *Archaeoglobus fulgidus* ferritin, hCAII: human carbonic anhydrase II, pNPA: 4-nitrophenyl acetate, pNP: 4-nitrophenol, SASA: solvent accessible surface area, SEC: Size

exclusion chromatography, DLS: Dynamic light scattering, CCS: carbon capture and storage, CCMV: cowpea chlorotic mottle virus, MWCO: molecular weight cutoff, LB, Luria broth

References

(1) Clark, J., and Macquarrie, D. (2007) Handbook of green chemistry and technology. *Handb. Green Chem. Technol.*

(2) Zaks, A., and Klibanov, A. M. (1984) Enzymatic catalysis in organic media at 100°C. *Science (80-.). 224*, 1249–51.

(3) Burton, S. G., Cowan, D. A., and Woodley, J. M. (2002) The search for the ideal biocatalyst. *Nat. Biotechnol. 20*, 37–45.

(4) Reetz, M. T. (2013) Biocatalysis in organic chemistry and biotechnology: Past, present, and future. *J. Am. Chem. Soc. 135*, 12480–12496.

(5) Arnold, F. H. (2018) Directed evolution: bringing new chemistry to life. *Angew. Chemie - Int. Ed. 57*, 4143–4148.

(6) Woodley, J. M. (2013) Protein engineering of enzymes for process applications. *Curr. Opin. Chem. Biol. 17*, 310–316.

(7) Turner, N. J., and O'reilly, E. (2013) Biocatalytic retrosynthesis. *Nat. Chem. Biol. 9*, 285–288.

(8) Sheldon, R. A., and Pereira, P. C. (2017) Biocatalysis engineering: The big picture. *Chem. Soc. Rev. 46*, 2678–2691.

(9) Denard, C. A., Ren, H., and Zhao, H. (2015) Improving and repurposing biocatalysts via

directed evolution. *Curr. Opin. Chem. Biol. 25*, 55–64.

(10) Sheldon, R. A., Brady, D., and Bode, M. L. (2020) The Hitchhiker's guide to biocatalysis: Recent advances in the use of enzymes in organic synthesis. *Chem. Sci. 11*, 2587–2605.

(11) Qu, G., Liu, B., Jiang, Y., Nie, Y., Yu, H., and Sun, Z. (2019) Laboratory evolution of an alcohol dehydrogenase towards enantioselective reduction of difficult-to-reduce ketones. *Bioresour. Bioprocess. 6*, 18.

(12) Nanda, V., Senn, S., Pike, D. H., Rodriguez-Granillo, A., Hansen, W. A., Khare, S. D., and Noy, D. (2016) Structural principles for computational and de novo design of 4Fe-4S metalloproteins. *Biochim. Biophys. Acta - Bioenerg. 1857*, 531–538.

(13) Rittle, J., Field, M. J., Green, M. T., and Tezcan, F. A. (2019) An efficient, step-economical strategy for the design of functional metalloproteins. *Nat. Chem. 11*, 434–441.

(14) Hayashi, T., Hilvert, D., and Green, A. P. (2018) Engineered metalloenzymes with non-canonical coordination environments. *Chem. - A Eur. J. 24*, 11821–11830.

(15) Lu, C., Shen, F., Wang, S., Wang, Y., Liu, J., Bai, W. J., and Wang, X. (2018) An engineered self-sufficient biocatalyst enables scalable production of linear α-olefins from carboxylic acids. *ACS Catal. 8*, 5794–5798.

(16) Stenner, R., Steventon, J. W., Seddon, A., and Anderson, J. L. R. (2020) A de novo peroxidase is also a promiscuous yet stereoselective carbene transferase. *Proc. Natl. Acad. Sci. U. S. A. 117*, 1419–1428.

(17) Fessner, N. D. (2019) P450 monooxygenases enable rapid late-stage diversification of natural products via C−H bond activation. *ChemCatChem 11*, 2226–2242.

(18) Seel, C. J., and Gulder, T. (2019) Biocatalysis fueled by light: On the versatile combination of photocatalysis and enzymes. *ChemBioChem 20*, 1871–1897.

(19) Li, P., Chen, Q., Wang, T. C., Vermeulen, N. A., Mehdi, B. L., Dohnalkova, A., Browning, N. D., Shen, D., Anderson, R., Gómez-Gualdrón, D. A., Cetin, F. M., Jagiello, J., Asiri, A. M., Stoddart, J. F., and Farha, O. K. (2018) Hierarchically engineered mesoporous metal-organic frameworks toward cell-free immobilized enzyme systems. *Chem 4*, 1022–1034.

(20) Chen, Y., Jiménez-Ángeles, F., Qiao, B., Krzyaniak, M. D., Sha, F., Kato, S., Gong, X., Buru, C. T., Chen, Z., Zhang, X., Gianneschi, N. C., Wasielewski, M. R., Olvera de la Cruz, M., and Farha, O. K. (2020) Insights into the enhanced catalytic activity of cytochrome c when encapsulated in a metal–organic framework. *J. Am. Chem. Soc. 142*, 18576–18582.

(21) Lee, C. H., Jin, E. S., Lee, J. H., and Hwang, E. T. (2020) Immobilization and stabilization of enzyme in biomineralized calcium carbonate microspheres. *Front. Bioeng. Biotechnol. 8*, 1191.

(22) Das, S., Zhao, L., Elofson, K., and Finn, M. G. (2020) Enzyme stabilization by virus-like particles. *Biochemistry 59*, 2870–2881.

(23) Guzik, U., Hupert-Kocurek, K., and Wojcieszyńska, D. (2014) Immobilization as a strategy for improving enzyme properties-application to oxidoreductases. *Molecules 19*, 8995–9018.

(24) Ma, C., Malessa, A., Boersma, A. J., Liu, K., and Herrmann, A. (2020) Supercharged proteins and polypeptides. *Adv. Mater. 32*, 1905309.

(25) Lawrence, M. S., Phillips, K. J., and Liu, D. R. (2007) Supercharging proteins can impart unusual resilience. *J. Am. Chem. Soc. 129*, 10110–10112.

(26) McNaughton, B. R., Cronican, J. J., Thompson, D. B., and Liu, D. R. (2009) Mammalian cell penetration, siRNA transfection, and DNA transfection by supercharged proteins. *Proc. Natl. Acad. Sci. U. S. A. 106*, 6111–6116.

(27) Miklos, A. E., Kluwe, C., Der, B. S., Pai, S., Sircar, A., Hughes, R. A., Berrondo, M., Xu, J., Codrea, V., Buckley, P. E., Calm, A. M., Welsh, H. S., Warner, C. R., Zacharko, M. A., Carney, J. P., Gray, J. J., Georgiou, G., Kuhlman, B., and Ellington, A. D. (2012) Structure-based design of supercharged, highly thermoresistant antibodies. *Chem. Biol. 19*, 449–455.

(28) Simeonov, P., Berger-Hoffmann, R., Hoffmann, R., Sträter, N., and Zuchner, T. (2011) Surface supercharged human enteropeptidase light chain shows improved solubility and refolding yield. *Protein Eng. Des. Sel. 24*, 261–268.

(29) Haarmeyer, C. N., Smith, M. D., Chundawat, S. P. S., Sammond, D., and Whitehead, T. A. (2017) Insights into cellulase-lignin non-specific binding revealed by computational redesign of the surface of green fluorescent protein. *Biotechnol. Bioeng. 114*, 740–750.

(30) Whitehead, T. A., Bandi, C. K., Berger, M., Park, J., and Chundawat, S. P. S. (2017) Negatively supercharging cellulases render them lignin-resistant. *ACS Sustain. Chem. Eng. 5*, 6247–6252.

(31) Johnson, L. B., Park, S., Gintner, L. P., and Snow, C. D. (2016) Characterization of supercharged cellulase activity and stability in ionic liquids. *J. Mol. Catal. B Enzym. 132*, 84–90.

(32) Pedersen, J. N., Zhou, Y., Guo, Z., and Pérez, B. (2019) Genetic and chemical approaches for surface charge engineering of enzymes and their applicability in biocatalysis: A review. *Biotechnol. Bioeng. 116*, 1795–1812.

(33) Cronican, J. J., Thompson, D. B., Beier, K. T., McNaughton, B. R., Cepko, C. L., and Liu, D. R. (2010) Potent delivery of functional proteins into mammalian cells in vitro and in vivo using a supercharged protein. *ACS Chem. Biol. 5*, 747–752.

(34) Wang, M., Zuris, J. A., Meng, F., Rees, H., Sun, S., Deng, P., Han, Y., Gao, X., Pouli, D., Wu, Q., Georgakoudi, I., Liu, D. R., and Xu, Q. (2016) Efficient delivery of genome-editing proteins using bioreducible lipid nanoparticles. *Proc. Natl. Acad. Sci. U. S. A. 113*, 2868–2873.

(35) Sasaki, E., Böhringer, D., Van De Waterbeemd, M., Leibundgut, M., Zschoche, R., Heck, A. J. R., Ban, N., and Hilvert, D. (2017) Structure and assembly of scalable porous protein cages. *Nat. Commun. 8*, 14663.

(36) Tetter, S., and Hilvert, D. (2017) Enzyme encapsulation by a ferritin cage. *Angew. Chemie - Int. Ed. 56*, 14933–14936.

(37) Rochelle, G. T. (2009) Amine scrubbing for CO2 capture. *Science (80-.). 325*, 1652–1654.

(38) Snæbjörnsdóttir, S. Ó., Sigfússon, B., Marieni, C., Goldberg, D., Gislason, S. R., and Oelkers, E. H. (2020) Carbon dioxide storage through mineral carbonation. *Nat. Rev. Earth Environ. 1*, 90–102.

(39) Singh, J., and Dhar, D. W. (2019) Overview of carbon capture technology: Microalgal biorefinery concept and state-of-the-art. *Front. Mar. Sci. 6*, 29.

(40) Qasem, N. A. A., Ben-Mansour, R., and Habib, M. A. (2018) An efficient CO2 adsorptive storage using MOF-5 and MOF-177. *Appl. Energy 210*, 317–326.

(41) Britt, D., Furukawa, H., Wang, B., Glover, T. G., and Yaghi, O. M. (2009) Highly efficient separation of carbon dioxide by a metal-organic framework replete with open metal sites. *Proc.*

Natl. Acad. Sci. U. S. A. 106, 20637–20640.

(42) Shao, L., Sang, Y., Huang, J., and Liu, Y. N. (2018) Triazine-based hyper-cross-linked polymers with inorganic-organic hybrid framework derived porous carbons for CO2 capture. *Chem. Eng. J. 353*, 1–14.

(43) Wang, W., Zhou, M., and Yuan, D. (2017) Carbon dioxide capture in amorphous porous organic polymers. *J. Mater. Chem. A 5*, 1334–1347.

(44) Basnayake, S. A., Su, J., Zou, X., and Balkus, K. J. (2015) Carbonate-based zeolitic imidazolate framework for highly selective co2 capture. *Inorg. Chem. 54*, 1816–1821.

(45) Krishnamurthy, V. M., Kaufman, G. K., Urbach, A. R., Gitlin, I., Gudiksen, K. L., Weibel, D. B., and Whitesides, G. M. (2008) Carbonic anhydrase as a model for biophysical and physical-organic studies of proteins and protein-ligand binding. *Chem. Rev. 108*, 946–1051.

(46) Effendi, S. S. W., and Ng, I. S. (2019) The prospective and potential of carbonic anhydrase for carbon dioxide sequestration: A critical review. *Process Biochem. 87*, 55–65.

(47) Vinoba, M., Bhagiyalakshmi, M., Jeong, S. K., Yoon, Y. I. I., and Nam, S. C. (2012) Immobilization of carbonic anhydrase on spherical SBA-15 for hydration and sequestration of CO 2. *Colloids Surfaces B Biointerfaces 90*, 91–96.

(48) Jing, G., Pan, F., Lv, B., and Zhou, Z. (2015) Immobilization of carbonic anhydrase on epoxy-functionalized magnetic polymer microspheres for CO2 capture. *Process Biochem. 50*, 2234–2241.

(49) Kanbar, B., and Ozdemir, E. (2010) Thermal stability of carbonic anhydrase immobilized within polyurethane foam. *Biotechnol. Prog. 26*, 1474–1480.

(50) Bilal, M., Asgher, M., Shahid, M., and Bhatti, H. N. (2016) Characteristic features and dye degrading capability of agar-agar gel immobilized manganese peroxidase. *Int. J. Biol. Macromol. 86*, 728–740.

(51) Min, K. H., Son, R. G., Ki, M. R., Choi, Y. S., and Pack, S. P. (2016) High expression and biosilica encapsulation of alkaline-active carbonic anhydrase for CO2 sequestration system development. *Chemosphere 143*, 128–134.

(52) Corchero, J. L., and Cedano, J. (2011) Self-assembling, protein-based intracellular bacterial organelles: Emerging vehicles for encapsulating, targeting and delivering therapeutical cargoes. *Microb. Cell Fact. 10*, 92.

(53) de Ruiter, M. V., van der Hee, R. M., Driessen, A. J. M., Keurhorst, E. D., Hamid, M., and Cornelissen, J. J. L. M. (2019) Polymorphic assembly of virus-capsid proteins around DNA and the cellular uptake of the resulting particles. *J. Control. Release 307*, 342–354.

(54) Matsuura, K. (2018) Synthetic approaches to construct viral capsid-like spherical nanomaterials. *Chem. Commun. 54*, 8944–8959.

(55) Seebeck, F. P., Woycechowsky, K. J., Zhuang, W., Rabe, J. P., and Hilvert, D. (2006) A simple tagging system for protein encapsulation. *J. Am. Chem. Soc. 128*, 4516–4517.

(56) Uchida, M., Kang, S., Reichhardt, C., Harlen, K., and Douglas, T. (2010) The ferritin superfamily: Supramolecular templates for materials synthesis. *Biochim. Biophys. Acta - Gen. Subj. 1800*, 834–845.

(57) Jutz, G., Van Rijn, P., Santos Miranda, B., and Böker, A. (2015) Ferritin: A versatile building block for bionanotechnology. *Chem. Rev. 115*, 1653–1701.

(58) Patterson, D. P., Prevelige, P. E., and Douglas, T. (2012) Nanoreactors by programmed enzyme encapsulation inside the capsid of the bacteriophage P22. *ACS Nano 6*, 5000–5009.

(59) Azuma, Y., Edwardson, T. G. W., and Hilvert, D. (2018) Tailoring lumazine synthase assemblies for bionanotechnology. *Chem. Soc. Rev. 47*, 3543–3557.

(60) Khoshnejad, M., Parhiz, H., Shuvaev, V. V., Dmochowski, I. J., and Muzykantov, V. R. (2018) Ferritin-based drug delivery systems: Hybrid nanocarriers for vascular immunotargeting. *J. Control. Release 282*, 13–24.

(61) Khoshnejad, M., Shuvaev, V. V., Pulsipher, K. W., Dai, C., Hood, E. D., Arguiri, E., Christofidou-Solomidou, M., Dmochowski, I. J., Greineder, C. F., and Muzykantov, V. R. (2016) Vascular accessibility of endothelial targeted ferritin nanoparticles. *Bioconjug. Chem. 27*, 628–637.

(62) Shuvaev, V. V., Khoshnejad, M., Pulsipher, K. W., Kiseleva, R. Y., Arguiri, E., Cheung-Lau, J. C., LeFort, K. M., Christofidou-Solomidou, M., Stan, R. V., Dmochowski, I. J., and Muzykantov, V. R. (2018) Spatially controlled assembly of affinity ligand and enzyme cargo enables targeting ferritin nanocarriers to caveolae. *Biomaterials 185*, 348–359.

(63) Macone, A., Masciarelli, S., Palombarini, F., Quaglio, D., Boffi, A., Trabuco, M. C., Baiocco, P., Fazi, F., and Bonamore, A. (2019) Ferritin nanovehicle for targeted delivery of cytochrome C to cancer cells. *Sci. Rep. 9*, 11749.

(64) Edwardson, T. G. W., Mori, T., and Hilvert, D. (2018) Rational engineering of a designed protein cage for siRNA delivery. *J. Am. Chem. Soc. 140*, 10439–10442.

(65) Palombarini, F., Fabio, E. Di, Boffi, A., Macone, A., and Bonamore, A. (2020) Ferritin

nanocages for protein delivery to tumor cells. *Molecules 25*, 825.

(66) Zhang, W., Xu, C., Yin, G. Q., Zhang, X. E., Wang, Q., and Li, F. (2017) Encapsulation of inorganic nanomaterials inside virus-based nanoparticles for bioimaging. *Nanotheranostics 1*, 358–368.

(67) Khoshnejad, M., Greineder, C. F., Pulsipher, K. W., Villa, C. H., Altun, B., Pan, D. C., Tsourkas, A., Dmochowski, I. J., and Muzykantov, V. R. (2018) Ferritin nanocages with biologically orthogonal conjugation for vascular targeting and imaging. *Bioconjug. Chem. 29*, 1209–1218.

(68) Chakraborti, S., Lin, T. Y., Glatt, S., and Heddle, J. G. (2020) Enzyme encapsulation by protein cages. *RSC Adv. 10*, 13293–13301.

(69) Brasch, M., Putri, R. M., De Ruiter, M. V., Luque, D., Koay, M. S. T., Castón, J. R., and Cornelissen, J. J. L. M. (2017) Assembling enzymatic cascade pathways inside virus-based nanocages using dual-tasking nucleic acid tags. *J. Am. Chem. Soc. 139*, 1512–1519.

(70) Azuma, Y., Bader, D. L. V., and Hilvert, D. (2018) Substrate sorting by a supercharged nanoreactor. *J. Am. Chem. Soc. 140*, 860–863.

(71) Schoonen, L., Nolte, R. J. M., and Van Hest, J. C. M. (2016) Highly efficient enzyme encapsulation in a protein nanocage: Towards enzyme catalysis in a cellular nanocompartment mimic. *Nanoscale 8*, 14467–14472.

(72) Schoonen, L., Maassen, S., Nolte, R. J. M., and Van Hest, J. C. M. (2017) Stabilization of a virus-like particle and its application as a nanoreactor at physiological conditions. *Biomacromolecules 18*, 3492–3497.

(73) Giessen, T. W., and Silver, P. A. (2016) A catalytic nanoreactor based on in vivo encapsulation of multiple enzymes in an engineered protein nanocompartment. *ChemBioChem 17*, 1931–1935.

(74) Lizatović, R., Assent, M., Barendregt, A., Dahlin, J., Bille, A., Satzinger, K., Tupina, D., Heck, A. J. R., Wennmalm, S., and André, I. (2018) A protein-based encapsulation system with calcium-controlled cargo loading and detachment. *Angew. Chemie - Int. Ed. 57*, 11334–11338.

(75) Quin, M. B., Perdue, S. A., Hsu, S. Y., and Schmidt-Dannert, C. (2016) Encapsulation of multiple cargo proteins within recombinant Eut nanocompartments. *Appl. Microbiol. Biotechnol. 100*, 9187–9200.

(76) Cassidy-Amstutz, C., Oltrogge, L., Going, C. C., Lee, A., Teng, P., Quintanilla, D., East-Seletsky, A., Williams, E. R., and Savage, D. F. (2016) Identification of a minimal peptide tag for in vivo and in vitro loading of encapsulin. *Biochemistry 55*, 3461–3468.

(77) Sutter, M., Boehringer, D., Gutmann, S., Günther, S., Prangishvili, D., Loessner, M. J., Stetter, K. O., Weber-Ban, E., and Ban, N. (2008) Structural basis of enzyme encapsulation into a bacterial nanocompartment. *Nat. Struct. Mol. Biol. 15*, 939–947.

(78) Putri, R. M., Allende-Ballestero, C., Luque, D., Klem, R., Rousou, K. A., Liu, A., Traulsen, C. H. H., Rurup, W. F., Koay, M. S. T., Castón, J. R., and Cornelissen, J. J. L. M. (2017) Structural characterization of native and modified encapsulins as nanoplatforms for in vitro catalysis and cellular uptake. *ACS Nano 11*, 12796–12804.

(79) Patterson, D. P., Schwarz, B., El-Boubbou, K., Van Der Oost, J., Prevelige, P. E., and Douglas, T. (2012) Virus-like particle nanoreactors: Programmed encapsulation of the

thermostable CelB glycosidase inside the P22 capsid. *Soft Matter 8*, 10158–10166.

(80) O'Neil, A., Prevelige, P. E., Basu, G., and Douglas, T. (2012) Coconfinement of fluorescent proteins: Spatially enforced communication of GFP and mCherry encapsulated within the P22 capsid. *Biomacromolecules 13*, 3902–3907.

(81) Sánchez-Sánchez, L., Tapia-Moreno, A., Juarez-Moreno, K., Patterson, D. P., Cadena-Nava, R. D., Douglas, T., and Vazquez-Duhalt, R. (2015) Design of a VLP-nanovehicle for CYP450 enzymatic activity delivery. *J. Nanobiotechnology 13*, 66.

(82) Kickhoefer, V. A., Garcia, Y., Mikyas, Y., Johansson, E., Zhou, J. C., Raval-Fernandes, S., Minoofar, P., Zink, J. I., Dunn, B., Stewart, P. L., and Rome, L. H. (2005) Engineering of vault nanocapsules with enzymatic and fluorescent. *Proc. Natl. Acad. Sci. U. S. A. 102*, 4348–4352.

(83) Pulsipher, K. W., Bulos, J. A., Villegas, J. A., Saven, J. G., and Dmochowski, I. J. (2018) A protein–protein host–guest complex: Thermostable ferritin encapsulating positively supercharged green fluorescent protein. *Protein Sci. 27*, 1755–1766.

(84) Johnson, E., Cascio, D., Sawaya, M. R., Gingery, M., and Schröder, I. (2005) Crystal structures of a tetrahedral open pore ferritin from the hyperthermophilic Archaeon Archaeoglobus fulgidus. *Structure 13*, 637–648.

(85) Pulsipher, K. W., and Dmochowski, I. J. (2014) Ferritin encapsulation and templated synthesis of inorganic nanoparticles, in *Protein Cages: Methods and Protocols*, pp 27–37.

(86) Cheung-Lau, J. C., Liu, D., Pulsipher, K. W., Liu, W., and Dmochowski, I. J. (2014) Engineering a well-ordered, functional protein-gold nanoparticle assembly. *J. Inorg. Biochem. 130*, 59–68.

(87) Swift, J., Butts, C. A., Cheung-Lau, J., Yerubandi, V., and Dmochowski, I. J. (2009) Efficient self-assembly of Archaeoglobus fulgidus ferritin around metallic cores. *Langmuir 25*, 5219–5225.

(88) Pulsipher, K. W., and Dmochowski, I. J. (2016) Ferritin: Versatile host, nanoreactor, and delivery agent. *Isr. J. Chem. 56*, 660–670.

(89) Chakraborti, S., Korpi, A., Kumar, M., Stępień, P., Kostiainen, M. A., and Heddle, J. G. (2019) Three-dimensional protein cage array capable of active enzyme capture and artificial chaperone activity. *Nano Lett. 19*, 3918–3924.

(90) Kim, C. S., Yang, Y. J., Bahn, S. Y., and Cha, H. J. (2017) A bioinspired dual-crosslinked tough silk protein hydrogel as a protective biocatalytic matrix for carbon sequestration. *NPG Asia Mater. 9*, e391.

(91) Jo, B. H., Seo, J. H., Yang, Y. J., Baek, K., Choi, Y. S., Pack, S. P., Oh, S. H., and Cha, H. J. (2014) Bioinspired silica nanocomposite with autoencapsulated carbonic anhydrase as a robust biocatalyst for CO2 sequestration. *ACS Catal. 4*, 4332–4340.

(92) Guo, H. H., Choe, J., and Loeb, L. A. (2004) Protein tolerance to random amino acid change. *Proc. Natl. Acad. Sci. U. S. A. 101*, 9205–9210.

(93) Rennell, D., Bouvier, S. E., Hardy, L. W., and Poteete, A. R. (1991) Systematic mutation of bacteriophage T4 lysozyme. *J. Mol. Biol. 222*, 67–86.

(94) Axe, D. D., Foster, N. W., and Fersht, A. R. (1998) A search for single substitutions that eliminate enzymatic function in a bacterial ribonuclease. *Biochemistry 37*, 7157–7166.

(95) Kono, H., and Saven, J. G. (2001) Statistical theory for protein combinatorial libraries.

Packing interactions, backbone flexibility, and the sequence variability of a main-chain structure. *J. Mol. Biol. 306*, 607–628.

(96) Swift, J., Wehbi, W. A., Kelly, B. D., Stowell, X. F., Saven, J. G., and Dmochowski, I. J. (2006) Design of functional ferritin-like proteins with hydrophobic cavities. *J. Am. Chem. Soc. 128*, 6611–6619.

(97) Butts, C. A., Swift, J., Kang, S.-G., Di Costanzo, L., Christianson, D. W., Saven, J. G., and Dmochowski, I. J. (2008) Directing noble metal ion chemistry within a designed ferritin protein. *Biochemistry 47*, 12729–12739.

(98) Diaz, J. E., Lin, C.-S., Kunishiro, K., Feld, B. K., Avrantinis, S. K., Bronson, J., Greaves, J., Saven, J. G., and Weiss, G. A. (2011) Computational design and selections for an engineered, thermostable terpene synthase. *Protein Sci. 20*, 1597–1606.

(99) Perez-Aguilar, J. M., Xi, J., Matsunaga, F., Cui, X., Selling, B., Saven, J. G., and Liu, R. (2013) A Computationally Designed Water-Soluble Variant of a G-Protein-Coupled Receptor: The Human Mu Opioid Receptor. *PLoS One 8*, e66009.

(100) Fraczkiewicz, R., and Braun, W. (1998) Exact and efficient analytical calculation of the accessible surface areas and their gradients for macromolecules. *J. Comput. Chem. 19*, 319–333.

(101) Behnke, C. A., Le Trong, I., Godden, J. W., Merritt, E. A., Teller, D. C., Bajorath, J., and Stenkamp, R. E. (2010) Atomic resolution studies of carbonic anhydrase II. *Acta Crystallogr. D. Biol. Crystallogr. 66*, 616–627.

(102) Calhoun, J. R., Kono, H., Lahr, S., Wang, W., DeGrado, W. F., and Saven, J. G. (2003) Computational design and characterization of a monomeric helical dinuclear metalloprotein. *J.*

Mol. Biol. 334, 1101–1115.

(103) Pulsipher, K. W., Villegas, J. A., Roose, B. W., Hicks, T. L., Yoon, J., Saven, J. G., and Dmochowski, I. J. (2017) Thermophilic ferritin 24mer assembly and nanoparticle encapsulation modulated by interdimer electrostatic repulsion. *Biochemistry 56*, 3596–3606.

(104) Shapovalov, M. V, and Dunbrack Jr, R. L. (2011) A smoothed backbone-dependent rotamer library for proteins derived from adaptive kernel density estimates and regressions. *Structure 19*, 844–858.

(105) Gasteiger, E., Hoogland, C., Gattiker, A., Duvaud, S., Wilkins, M. R., Appel, R. D., and Bairoch, A. (2005) Protein identification and analysis tools on the ExPASy server, in *The Proteomics Protocols Handbook*, pp 571–607.

(106) Wang, Y., Roose, B. W., Philbin, J. P., Doman, J. L., and Dmochowski, I. J. (2016) Programming A molecular relay for ultrasensitive biodetection through 129XeNMR. *Angew. Chemie - Int. Ed. 55*, 1733–1736.

(107) Anderson, J., Byrne, T., Woelfel, K. J., Meany, J. E., Spyridis, G. T., and Pocker, Y. (1994) The hydrolysis of p-nitrophenyl acetate: A versatile reaction to study enzyme kinetics. *J. Chem. Educ. 71*, 715.

(108) Khalameyzer, V., Fischer, I., Bornscheuer, U. T., and Altenbuchner, J. (1999) Screening, nucleotide sequence, and biochemical characterization of an esterase from Pseudomonas fluorescens with high activity towards lactones. *Appl. Environ. Microbiol. 65*, 477–482.

(109) Avvaru, B. S., Kim, C. U., Sippel, K. H., Gruner, S. M., Agbandje-McKenna, M., Silverman, D. N., and McKenna, R. (2010) A short, strong hydrogen bond in the active site of

human carbonic anhydrase II. *Biochemistry 49*, 249–251.

(110) Hovmöller, S., Zhou, T., and Ohlson, T. (2002) Conformations of amino acids in proteins. *Acta Crystallogr. Sect. D Biol. Crystallogr. D58*, 768–776.

(111) Jurrus, E., Engel, D., Star, K., Monson, K., Brandi, J., Felberg, L. E., Brookes, D. H., Wilson, L., Chen, J., Liles, K., Chun, M., Li, P., Gohara, D. W., Dolinsky, T., Konecny, R., Koes, D. R., Nielsen, J. E., Head-Gordon, T., Geng, W., Krasny, R., Wei, G.-W., Holst, M. J., McCammon, J. A., and Baker, N. A. (2018) Improvements to the APBS biomolecular solvation software suite. *Protein Sci. 27*, 112–128.

(112) Humphrey, W., Dalke, A., and Schulten, K. (1996) VMD: Visual molecular dynamics. *J. Mol. Graph. 14*, 33–38.

(113) Comellas-Aragonès, M., Engelkamp, H., Claessen, V. I., Sommerdijk, N. A. J. M., Rowan, A. E., Christianen, P. C. M., Maan, J. C., Verduin, B. J. M., Cornelissen, J. J. L. M., and Nolte, R. J. M. (2007) A virus-based single-enzyme nanoreactor. *Nat. Nanotechnol. 2*, 635–639.

(114) Zucca, P., Fernandez-Lafuente, R., and Sanjust, E. (2016) Agarose and its derivatives as supports for enzyme immobilization. *Molecules 21*.

(115) Lian, X., Erazo-Oliveras, A., Pellois, J.-P., and Zhou, H.-C. (2017) High efficiency and long-term intracellular activity of an enzymatic nanofactory based on metal-organic frameworks. *Nat. Commun. 8*, 2075.

(116) Gawande, P. V, and Kamat, M. Y. (1998) Preparation, characterization and application of Aspergillus sp. xylanase immobilized on Eudragit S-100. *J. Biotechnol. 66*, 165–175.

(117) Mazlan, S. Z., and Hanifah, S. A. (2017) Effects of temperature and pH on immobilized

laccase activity in conjugated methacrylate-acrylate microspheres. *Int. J. Polym. Sci.* (Schnabelrauch, M., Ed.) *2017*, 5657271.

(118) Homaei, A. A., Sajedi, R. H., Sariri, R., Seyfzadeh, S., and Stevanato, R. (2010) Cysteine enhances activity and stability of immobilized papain. *Amino Acids 38*, 937–942.

For Table of Contents use only